





Thermosuperrepellency of a hot substrate caused by vapour percolation

J. Benedikt Schmidt ¹, Julian Hofmann¹, Fabian M. Tenzer¹, Jan Breitenbach ¹, Cameron Tropea ¹ & Ilia V. Roisman ¹✉

Drop rebound after collision with a very hot substrate is usually attributed to the Leidenfrost effect, characterized by intensive film boiling in a thin vapour gap between the liquid and substrate. Similarly, drop impact onto a cold superhydrophobic substrate leads to a complete drop rebound, despite partial wetting of the substrate. Here we study the repellent properties of hot smooth hydrophilic substrates in the nucleate boiling, non-Leidenfrost regime and discover that the thermally induced repellency is associated with vapour percolation on the substrate. The wetting structure in the presence of the percolating vapour rivulets is analogous to the Cassie-Baxter wetting mode, which is a necessary condition for the repellency in the isothermal case. The theoretical predictions for the threshold temperature for vapour percolation agree well with the experimental data for drop rebound and correspond to the minimum heat flux when spray cooling.

¹Technische Universität Darmstadt, Institute for Fluid Mechanics and Aerodynamics, Darmstadt, Germany. ✉email: roisman@sla.tu-darmstadt.de

In describing drop interaction with solid surfaces, researchers have reverted (unknowingly) to endowing drops and surfaces with the ability to empathize—drops spread with love on friendly hydrophilic substrates (the word hydrophilic is formed from the ancient Greek words ὕδωρ and φίλια for water and love.). In contrast, drops impacting onto a fearful hydrophobic (from the Greek ὑδρόφοβος, terrified by water) or even superhydrophobic surfaces can often lead to rebound. What then does a drop “feel” when impacting onto an extremely hot substrate? Thermally induced drop rebound is one of the numerous observed impact outcomes^{1–3}, which also include deposition, evaporation, breakup and atomization. These phenomena are substantially more complex and have to be described combining the hydrodynamic and thermodynamic aspects of the drop boiling on a hot substrate.

Drop spreading after impact onto a solid dry substrate is governed by the impact Reynolds number ($Re \equiv \rho d_0 U_0 / \mu$) and the Weber number ($We \equiv \rho d_0 U_0^2 / \sigma$), where ρ , μ , and σ are the density, viscosity, and surface tension of the liquid, d_0 is the initial drop diameter and U_0 is the impact velocity. Drop collision in the absence of thermal effects leads to the generation of a thin radially spreading lamella, bounded by a rim, formed by surface tension and the forces associated with the substrate wetting properties^{4,5}.

Immediately after impact, an expanding viscous boundary layer of thickness $\sim \sqrt{\nu t}$ is formed in the vicinity of the wall, where ν is the kinematic viscosity of the liquid and t the time after impact. At some instant the thickness of the viscous boundary layer is equal to the lamella thickness. At subsequent times the flow in the lamella is quickly damped by the viscosity. The theoretically predicted residual lamella thickness and the characteristic time of spreading governed by viscosity are obtained in the form⁶

$$h_{\text{res}} \approx 0.79 d_0 Re^{-2/5}, t_\nu = \frac{d_0 Re^{1/5}}{U_0}. \quad (1)$$

For lower Weber number the effect of surface tension becomes dominant and the rim can start to recede before the cessation of the flow in the lamella. In many cases, for example in the film boiling regime⁷, in the case of drop impact onto a superhydrophobic substrate^{8–11}, or binary drop collisions¹², the spreading time is scaled very well with the typical time of drop natural oscillations

$$t_\sigma \approx \sqrt{\frac{\rho d_0^3}{\sigma}} = \frac{d_0 We^{1/2}}{U_0}. \quad (2)$$

The viscous spreading regime corresponds to the case $t_\nu \ll t_\sigma$, namely when $We \gg Re^{2/5}$.

In the case of drop impact onto a hot substrate, two thermal boundary layers, in the solid substrate and in the liquid flow, start to expand in the vicinity of the liquid/solid interface¹³. If the substrate initial temperature T_{wall} is well above the saturation point T_{sat} , the flow is accompanied by the heterogeneous nucleation of the vapor bubbles^{14,15}. In this regime the wall temperature near the evaporating contact line of each bubble approaches T_{sat} . The heat flux \dot{q} in the nucleate boiling regime is then estimated¹⁶ from the well-known solution of the conduction problem in the wall

$$\dot{q} = \frac{e_w \Delta T_w}{\sqrt{\pi t}}. \quad (3)$$

The total evaporation time of the deposited drop can now be estimated using Eq. (3) from the balance of the total heat required for the complete drop evaporation and the heat transferred from

the substrate¹⁶

$$t_{\text{cdrop}} = \pi \left(\frac{\rho L^* d_0}{12 k_w e_w \Delta T_w} \right)^2, \Delta T_w = T_{\text{wall}} - T_{\text{sat}}, \quad (4)$$

in which k_w is a dimensionless empirical constant of the order of unity, associated with the surface wettability, e_w is the thermal effusivity of the substrate and $L^* = L + \Delta H_0$ is the sum of the latent heat of evaporation L and the enthalpy difference ΔH_0 between the initial drop and saturated liquid.

In this experimental and theoretical study, we demonstrate that the relations of the main time scales (the capillary time, the viscous time and the typical time for drop evaporation) determine the observed outcome of drop impact onto a hot substrate. Moreover, we demonstrate that the drop rebound is not necessarily associated with the film boiling regime and the threshold temperature of the drop rebound is therefore not always equal to the Leidenfrost point.

Results and discussion

Observed phenomena. Typical phenomena of drop impact onto a substrate at various initial temperatures, captured using a high-speed video system, are shown in Fig. 1a–c. The contact residence time t_r of an impacting drop is determined either by the instant of drop rebound or by the duration of complete evaporation of a deposited drop and is shown in Fig. 1d as a function of the initial substrate overhear $T_{\text{wall}} - T_{\text{sat}}$. Three main outcomes of drop impact accompanied by boiling include drop deposition with complete evaporation (one example is shown in Fig. 1a), complete or in some cases partial rebound after a certain delay due to a short period of sticking to the substrate (illustrated by the example in Fig. 1b), and non-sticking rebound (Fig. 1c). These results are similar to the recently published observations of drop impact¹⁷. The observations of the drop impact outcome cannot always unequivocally indicate a certain microscopic thermodynamic phenomenon at the substrate: nucleate, transitional or film boiling.

As shown in the graph in Fig. 1d, the contact residence time t_r of the deposited drop for $\Delta T_{\text{wall}} < 50^\circ\text{C}$ marked by the yellow color, agrees well with the theoretical predictions in Eq. (4) developed for nucleate boiling. In the range of highest wall temperatures ($\Delta T_w > 100^\circ\text{C}$, pink region in Fig. 1) the residence time is very close to the drop capillary time t_σ defined in Eq. (2) due to the non-sticking drop rebound. In this temperature range the drop is still in contact with the substrate as shown in literature¹⁷. However, in the intermediate range of the temperatures ($50^\circ\text{C} < \Delta T_w < 100^\circ\text{C}$) the residence time t_r deviates significantly from both t_{cdrop} and t_σ . The delay of the drop rebound in this regime is caused by the bonding of the drop at residual wetted spots of the target, as in the 10 ms frame in Fig. 1b.

In Fig. 2 the results of the measurements of t_r on the steel target are also shown in comparison with the theoretically predicted times t_{cdrop} and t_σ . While in Fig. 2a the residence time for a certain set of impact parameters are shown, in Fig. 2b the value of t_r is shown averaged over a substrate temperature class. For the steel target the regime of the good agreement of the residual time with t_{cdrop} is observed in the range $\Delta T_{\text{wall}} < 100^\circ\text{C}$, which is significantly wider than the range observed for aluminum targets (see Fig. 1). Therefore, the residence time is significantly influenced by the thermal properties of the substrate, its initial temperature as well as by the impact parameters.

Let us denote T^* as the lowest wall temperature at which the drop does not stick to the substrate. This point corresponds to the local minimum in the total heat, $Q = \int_0^{t_r} A(t) \dot{q}(t) dt$ transferred from the substrate during drop impact, since the heat increases

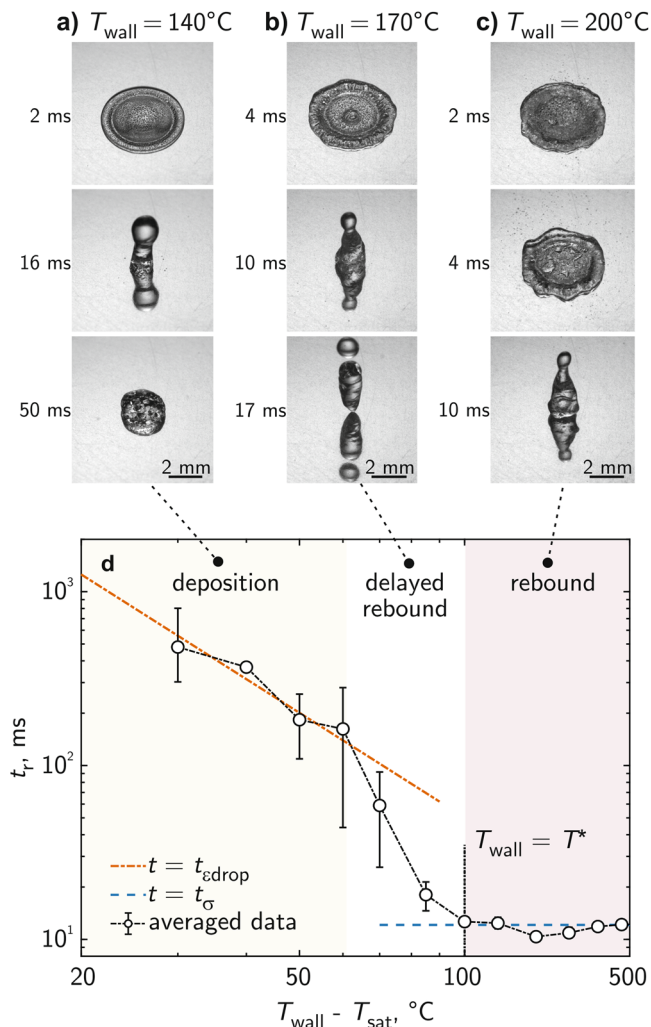


Fig. 1 Typical stages and main outcomes of drop impact onto a hot solid substrate at various initial temperatures. The figure shows a water drop with an initial drop diameter $d_0 = 2.35$ mm impacting onto an aluminum substrate with the impact velocity $U_0 = 0.7$ m s⁻¹. **a**, **b**, and **c** are exemplary images of drop impacts captured using a high-speed video system. All images are top view observations at an angle of 60° to the surface. **a** Drop impact at initial substrate temperature of $T_{\text{wall}} = 140$ °C shows drop spreading, receding, and deposition in the nucleate boiling regime. The contact residence time is determined by complete drop evaporation; **b** $T_{\text{wall}} = 170$ °C intensive nucleate boiling leads to the drop rebound delayed by a short period of sticking (see the image at 10 ms); **c** $T_{\text{wall}} = 200$ °C, non-sticking drop rebound; **d** Dependence of the average contact residence time t_r on the wall overheat temperature $T_{\text{wall}} - T_{\text{sat}}$ in comparison with the theoretical estimations for the total evaporation time of a deposited drop t_{edrop} and the drop natural oscillation time t_σ . Each point is the average value for experimental determined residence times in the corresponding temperature class. The error bars show the minimum and maximum observed residence times during experiments.

with the residence time and with the wall temperature. Here $A(t)$ is the wetted area of the substrate. We can thus expect that the heat flux during spray cooling at the threshold point T^* will also be minimal.

In Fig. 3a, the evolution of the heat flux \dot{q} and the interface temperature T_i of a thick stainless steel target continuously cooled by spray impact are shown. The target is initially heated uniformly up to $T_w \approx 450$ °C. The high-speed observations of spray impact, shown in the inserts in Fig. 3a, demonstrate that the

threshold temperature T^* associated with the minimum of the heat flux curve indeed determines the deposition/rebound limit for the impacting drops.

The value of the threshold temperature T^* depends neither on the drop diameter in the spray nor on the impact velocity, but on the target material, as is demonstrated in Fig. 3b, c. Moreover, no dependence of the temperature T^* on the mass flux of the impacting spray or other impact properties has been identified.

Drop boiling on a hot substrate. In Fig. 4 details are shown of the development of the vapor phase in the advanced nucleate boiling regime, which allow us to better understand the mechanisms of a single drop rebound. Figure 4a clearly shows the vapor bubbles on the aluminum substrate at $T_{\text{wall}} = 170$ °C and in b the formation of elongated vapor rivulets at higher temperatures, $T_{\text{wall}} = 200$ °C, at which drops rebound without delay. The impact parameters in Fig. 4a, b are the same as in Fig. 1. Figure 4c is the map of the heat flux distribution at the surface of a transparent sapphire target at $T_{\text{wall}} = 378$ °C during drop spreading (see Table 1). The wall temperature is well above the threshold temperature T^* . The red spots, corresponding to high local heat flux, indicate wetting of the substrate. The green or blue regions of low heat flux indicate the percolated vapor rivulets, similar to those observed in Fig. 4b. The same phenomena of vapor rivulets and cluster have been observed during drop impacts of ethanol drops onto sapphire substrate with TIR measurements in the same drop impact regime¹⁷.

The randomly distributed disks on a plane in Fig. 4d is an exemplary illustration of the irregular nucleation of bubbles on a solid surface. The spatial distribution of disks is characterized by the cumulative relative area λ of the disks, scaled by the total area of the domain. Some of the discs intersect and thus form clusters of disks. The distribution of the cluster sizes is studied in the framework of the percolation theory. The percolation threshold in this two-dimensional problem¹⁸ is $\lambda_c = 1.128$. At this point an infinite cluster of the intersecting disks first appears, as shown in Fig. 4d. The formation of the wrapping cluster of the disks at the percolation threshold can explain the percolation of the vapor bubbles and formation of the vapor rivulets. At the percolation threshold the liquid area of drop/substrate contacts are isolated spots. This situation is analogous to the Cassie-Baxter wetting of heterogeneous substrates, associated with the superhydrophobicity and superrepellency¹⁹ in conventional, isothermal cases.

The computed value $\lambda_c = 1.128$ is only a very rough approximation for the percolation threshold for the vapor bubbles, since the model does not consider bubble coalescence or shear driven motion of the bubbles in the liquid flow.

The relative wetted surface area (not belonging to the surface covered by the bubbles) is, ϵ , derived using the Poisson distribution of the expected number of bubbles covering a given point of the surface²⁰, assuming a random spatial distribution of bubble centers. At the percolation threshold it yields

$$\epsilon_c = \exp(-\lambda_c) \approx 0.32. \tag{5}$$

Heat transfer in the wall during nucleate boiling of a drop. The flow in the drop for values of relative volume of the liquid phase $\epsilon < \epsilon_c$ is completely different since the liquid contacts the substrate only at isolated wetted spots, which cannot prevent drop rebound, as in Fig. 1c. Let us roughly estimate the wall temperature corresponding to the emergence of the percolating vapor channels during the spreading time t_σ .

Consider the liquid lamella of the thickness h_{res} defined in Eq. (1). It can be estimated from the one-dimensional energy balance

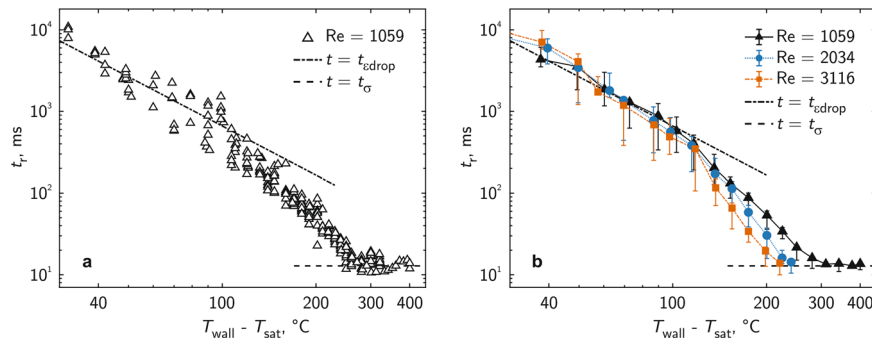


Fig. 2 Parametric study of the residence time of an impacting water drop on a hot steel target. **a** Experimental results on the residence time t_r of impacting drops with a Reynolds number $Re \equiv \rho d_0 U_0 / \mu = 1054$, with ρ and μ being the liquid density and viscosity, d_0 the initial drop diameter and U_0 the impact velocity. Each symbol corresponds to a single drop impact onto a steel target with various initial temperatures. The impact parameters are $d_0 = 2.3$ mm and $U_0 = 0.46$ m s⁻¹. The experimental data are compared to theoretical estimations of the total evaporation time of a deposited drop t_{edrop} and natural oscillation time t_σ . **b** Residence time t_r averaged over a target temperature class for different impact velocities. Each experimental point is the average value of ten experiments for the corresponding temperature class. The error bars represent one standard deviation $\pm s$. The experimental residence time is shown in comparison to the theoretical models t_{edrop} and t_σ .

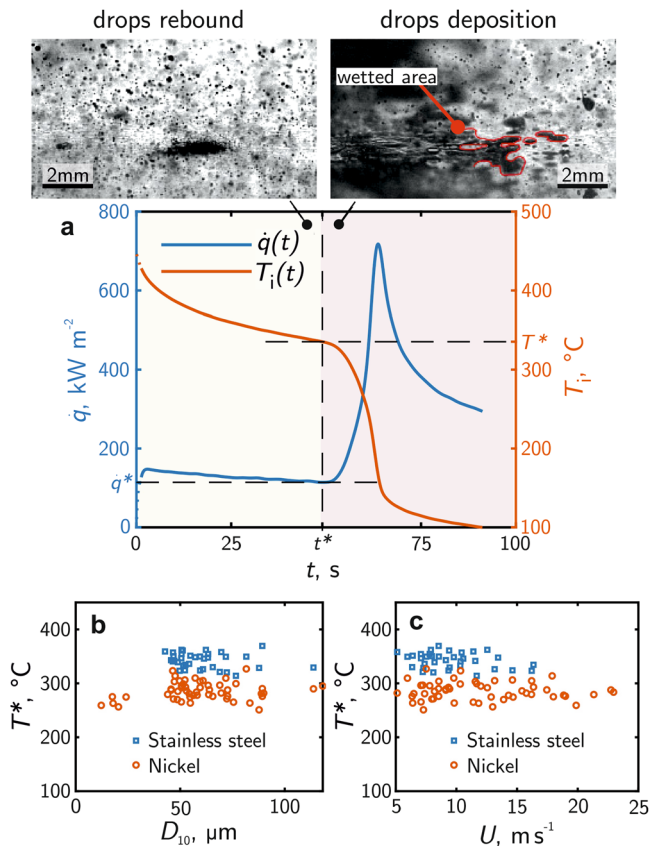


Fig. 3 The threshold temperature T^* for spray impact. **a** Exemplary results for the evolution of the heat flux \dot{q} and surface temperature T_i as a function of time t for spray cooling with distilled water. The threshold temperature T^* at the instant t^* corresponds to the minimum heat flux. Inserts show liquid patterns on the surface shortly above and below the threshold temperature T^* . **b** and **c** The dependence of the threshold temperature T^* on the average drop diameter D_{10} in the spray and on the average impact velocity U , respectively. Each point represents the threshold temperature T^* of a spray cooling experiment, as shown in **a**.

accounting for the creation of the vapor phase, expressed as

$$\rho h_{res} L^* \epsilon'(t) = -\dot{q}, \tag{6}$$

where ϵ is the relative volume of the liquid phase in the lamella.

The heat flux \dot{q} at the wall surface, determined in Eq. (3), is governed by the heat conduction in the thermal boundary layer in the wall. This expression allows to predict very well the heat flux during spray cooling in the nucleate boiling regime in a wide range of spray parameters and wall temperatures²¹. Therefore, the presence of bubbles does not influence the value of \dot{q} significantly. In a steady heat conduction in the wall, the presence of bubbles leads to local disturbances of the temperature field, but the total heat flux at the interface remains the same due to the energy balance. The heat flux can only be changed if transient effects, associated with bubble growth are significant²². The size of the wall region, disturbed by the presence of a bubble is comparable with the bubble radius. Therefore, the contribution of the bubbles presence at the substrate surface is small if the bubble size is much smaller than the thickness of the thermal boundary layer in the wall. This condition is satisfied in our experiments.

The solution of the ordinary differential equation in Eq. (6) is

$$\epsilon(t) = 1 - \frac{1.43 e_w \Delta T_w Re^{2/5} t^{1/2}}{\rho d_0 L^*}. \tag{7}$$

With the help of Eqs. (2), (3), and (5) the condition $\epsilon = \epsilon_c$ at the instant $t = t_\sigma$ yields the following expression for the threshold overhear ΔT in the surface tension driven spreading regime

$$\Delta T = b \Delta T_\sigma, \Delta T_\sigma = \frac{d_0^{1/4} L^* \rho^{3/4} \sigma^{1/4}}{e_w Re^{2/5}}, \tag{8}$$

where $b = 0.48$ and ΔT_σ is a typical scale for the threshold overhear in the surface tension dominated drop impact regime.

It should be noted that the coefficient b can be influenced by the reduction of the wetted area of the drop due to the appearance of dry spots, due to the liquid flow in the lamella, drop atomization and other factors. Therefore, the solution Eq. (8) is not exact. However, in this study it is important that the factor b in Eq. (8) has to be comparable with unity if the major physical factors are taken into account correctly.

For very high Weber numbers the duration of drop spreading is scaled by the viscous time scale t_v , defined in Eq. (1). The percolation condition $\epsilon = \epsilon_c$ at the instant $t = t_v$ yields another expression for the threshold wall overhear ΔT_v in the viscous

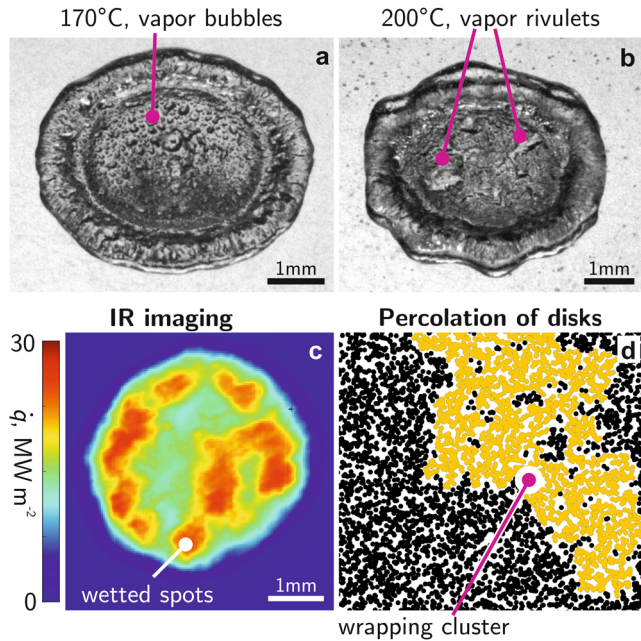


Fig. 4 Boiling of the liquid lamella on a hot substrate. **a** Spreading of a drop on a polished aluminum substrate at a initial substrate temperature $T_{wall} = 170\text{ }^\circ\text{C}$ in the delayed rebound regime, captured by the high-speed video system from the top. Bubbles are the result of the heterogeneous nucleation at the substrate. **b** Appearance of the percolating vapor rivulets during spreading of a drop on a polished aluminum substrate at $T_{wall} = 200\text{ }^\circ\text{C}$. This impact leads to a non-sticking rebound. **c** Heat flux map, computed using the images captured using the high-speed infrared camera during drop impact onto a sapphire target at $T_{wall} = 378\text{ }^\circ\text{C}$, corresponding to the non-sticking rebound accompanied by the intensive generation of fine secondary drops. The red regions of peak heat flux correspond to the substrate wetting. **d** Visualization of a continuum percolation with randomly distributed disks at a cumulative disk area $\lambda = 1.2$, slightly above the percolation threshold $\lambda_c = 1.128$. Each disk represents a simplified nucleation bubble. Above the percolation threshold, the bubbles wrap to large clusters as marked by the orange color in **d** and shown in **b** and **c**.

spreading regime

$$\Delta T_\nu = \frac{\rho\sqrt{\nu}L^*}{e_w} \tag{9}$$

In our estimation of heat transfer Eq. (6) the relative wetted surface area ϵ is approximated by the liquid volume fraction and the residual thickness h_{res} is assumed to be constant. This assumption cannot be very precise if the height of the vapor bubbles/channels changes in time, for example due to the evaporation of the drop lamella. Our analysis is therefore valid for the cases when the $t_\sigma \ll t_{edrop}$. This condition is satisfied for drop impacts at the threshold temperature, as shown in Fig. 1. The recent direct observations of the relative liquid contact area¹⁷ can potentially help to determine the relation to the volume fraction. These data could be a topic of interesting future investigations.

The expression for ΔT_ν does not depend on the drop diameter or impact velocity. This is not surprising, since the time t_ν and the lamella thickness h_{res} correspond to the one-dimensional growth of the viscous boundary layer in the lamella.

In Fig. 5, the theoretically predicted scales for the threshold temperature ΔT_σ and ΔT_ν are compared with the experimental data. The data for low-speed impacts with $We < 2.5 Re^{2/5}$, governed by surface tension, are shown in Fig. 5a as a function

of ΔT_σ . The factor 2.5 is empirical, determined from numerous experiments. The agreement is good, considering that the target materials and the impact velocities have been widely varied in the experiments.

The slope for spray impact is, however, larger than for a single drop, since the thermodynamic processes in the spreading drop are influenced significantly by the flow, although the expressions for the viscous length scale and for the time scale of capillary oscillations remain the same. In the case of spray cooling, shown in Fig. 5b, the values for ΔT^* are determined from the condition of the minimum of the heat flux. Note also that in the spray case the surface temperature is not uniform and is not continuous since it is influenced by single drop impacts. Each drop impact leads to a significant local cooling of a substrate. The subsequent drop with some probability, depending on the spray flux, could impact onto this relatively cold spot and thus initiate a wetted boiling region. This phenomenon has been recently identified using the high-speed video observations of spray impact onto very hot substrates²¹. The nucleate boiling in these wetted regions contribute significantly to the heat flux. The only average in time and space surface temperature has been determined in the spray cooling experiments, shown in Fig. 5b.

Moreover, the threshold temperature during spray cooling can also be influenced by the thermal atomization phenomenon associated with the drop levitation when the thermal boundary layer reaches the free surface of the drop spreading lamella²³. It can be shown with the help of Eq. (1) that the residence time t_θ of the thermal atomization regime is

$$t_\theta = t_\nu Pr, \tag{10}$$

where Pr is the Prandtl number characterizing the drop liquid. Some influence of the Prandtl number on the slope of the linear dependence of ΔT^* on ΔT_ν can thus be expected in the cases when the effect of thermal atomization is significant. Such an effect can only be identified in experiments of spray cooling with different liquids.

Several hypotheses have been put forward in the literature to explain the mechanism of film boiling. Some theoretical models have been developed based on the hydrodynamic stability analysis of the vapor/liquid interface^{24,25} or thermocapillary stability²⁶. Other authors assume that the Leidenfrost temperature is determined by the foam limit^{27,28} or by the limiting minimum vapor thickness²⁹ comparable with the surface roughness. In this study, we have demonstrated that the transition to the film boiling regime is initiated at the threshold point for vapor percolation. Further drop evaporation is governed by the presence of the vapor rivulets and is characterized by the disappearance of the isolated wetted spots. The film boiling regime corresponds to a complete vanishing of the wetted spots.

Methods

Two main experimental setups are used to observe single drop impact and to characterize spray cooling of hot substrates. They are shown schematically in Fig. 6.

Observations of single-drop impact onto a hot substrate. Two configurations of the experimental setup for a single drop impact are used in this study. One is to study the outcome of drop impact onto metal targets (Fig. 6a) and the other is for the high-speed thermographic visualization of the substrate interface exposed to the collision of a drop (Fig. 6b).

In both setups single drops of double-distilled water with a diameter of $d_0 = 2.3\text{ mm}$ are generated by a drop generator (as shown in Fig. 6a). A Bartels micro pump mp6 feeds a hydrophobic G27 blunt needle. The drop is released when the gravitational force exceeds the force due to the surface tension of the liquid. This principle leads to very constant drop diameters. The needle of the drop generator is cooled to maintain the liquid temperature constant at $20\text{ }^\circ\text{C}$. By changing the height of the needle above the substrate, the impact velocity can be changed in the range of $U_0 = 0.4\text{ to }2\text{ m s}^{-1}$. Various target materials are used to identify the influence of the material properties on the drop impact outcome: aluminum (EN

Table 1 List of the liquid and substrate materials and the values of the threshold temperature T^* .

Source	Type of experiment	Fluid	Substrate material	Thermal effusivity $e_w \text{ W s}^{1/2} \text{ m}^{-2} \text{ K}^{-1}$	$T^* \text{ }^\circ\text{C}$
This study	Spray	Water	Stainless steel 1.4841	8.8501×10^3	342
This study	Spray	Water	Nickel 2.4068	1.7892×10^4	286
32	Spray	Water	Stainless steel 1.4301	9.0193×10^3	371
33	Spray	Water	Nickel	1.8569×10^4	321
34	Spray	Water	Copper	3.6476×10^4	134
35	Spray	Water	Copper with chrome plating	1.7831×10^4	222
36	Spray	Water	Copper with chrome plating	1.7831×10^4	253
37	Spray	Water	Copper with chrome plating	1.7831×10^4	266
38	Drop chain	Water	Copper with gold plating	2.7701×10^4	225
This study	Drop	Water	Stainless steel 1.4841	8.8501×10^3	410
This study	Drop	Water	Stainless steel 1.4841	8.8501×10^3	370
This study	Drop	Water	Stainless steel 1.4841	8.8501×10^3	325
This study	Drop	Water	Stainless steel 1.4841	8.8501×10^3	320
This study	Drop	Water	Aluminum	2.5040×10^4	248
This study	Drop	Water	Aluminum	2.5040×10^4	221
This study	Drop	Water	Aluminum	2.5040×10^4	211
This study	Drop	Water	Copper	3.6853×10^4	172
This study	Drop	Water	Copper	3.6853×10^4	158
39	Drop	Water	Silicon wafer	9.7544×10^3	480
28	Drop	Water	FeCrAl	6.5664×10^3	445
28	Drop	Water	Sintered SiC	1.5733×10^4	350
28	Drop	Water	Zr-4	5.1511×10^3	531

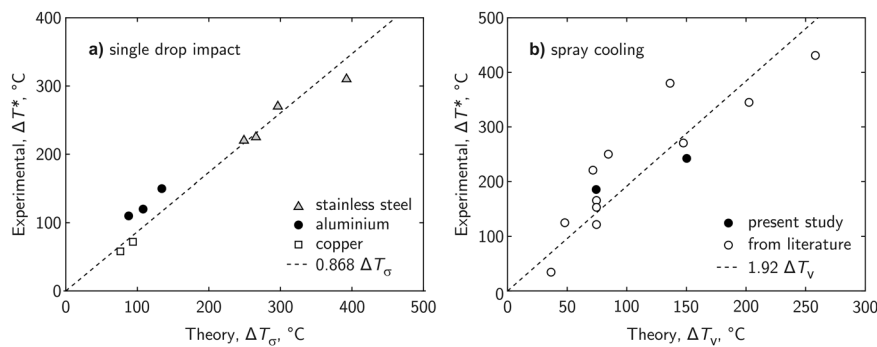


Fig. 5 Comparison of the threshold overheat temperatures ΔT^* , with the theoretically predicted scales of the threshold overheat ΔT_σ and ΔT_v . The experimental threshold overheat $\Delta T^* \equiv T^* - T_{\text{sat}}$ is defined as threshold temperature T^* from which on the residence time t_r is constant and single drops rebound. In spray cooling experiments the threshold temperature T^* is determined by the temperature of minimum heat flux. T_{sat} is the liquid boiling temperature. In **a** the experimental data of ΔT^* are compared for different substrate materials and impact parameters with ΔT_σ defined in Eq. (8). Single drop impacts are in the surface tension driven regime with $We < 2.5 \text{ Re}^{2/5}$. The Reynolds number is $\text{Re} \equiv \rho d_0 U_0 / \mu$ and the Weber number $We \equiv \rho d_0 U_0^2 / \sigma$, where ρ is the density, μ viscosity and σ surface tension of the liquid, d_0 the initial drop diameter and U_0 the impact velocity. Each Threshold temperature is determined by a series of single drop experiments with constant impact parameters. In **b**, experimental data and data from literature for spray cooling of targets of different materials and for the high-speed single drop impacts with $We > 2.5 \text{ Re}^{2/5}$, governed by viscosity are compared with ΔT_v . The data for different substrate materials for this study and from the literature are listed in Table 1. The data from the present study are averaged for each substrate material, since ΔT_v is independent on spray parameters.

AW 7075), copper (CW004A) or stainless steel (1.4841). The surface of all impact targets are mirror polished (surface roughness $S_a = 0.0108 \mu\text{m}$). The replaceable impact substrates are heated by a custom heating device with a total heating power of 400 W. The surface temperature is measured with a type J thermocouple (class 1) 1 mm below the surface. The drop impact is observed using a high-speed video system, consisting of a CMOS camera (Phantom V12.1) with a telecentric lens (Opto engineering TC16M036) and background illumination (Opto engineering LTCLHP036-G).

The setup for the visualization of the micro-scale thermodynamic effects at the drop-substrate interface and for the measurements of the temperature distribution is shown in Fig. 6b. A 3 mm thick, infrared (IR) transparent sapphire target which is coated on top with a 600 nm thick highly infrared emissive CrN PVD layer is used as an impact target. The IR radiation of the coating is captured through the transparent substrate with a mid-wave infrared camera (FLIR x6901sc) during the drop impact experiments.

An in-situ calibration is performed to convert the captured IR radiation into the surface temperature. During the calibration a copper block is placed at the coated

surface and both, the copper block as well as the heating structure are heated to the same temperature to provide a homogeneous temperature at the impact surface. A type J thermocouple (class 1) is placed 0.5 mm above the copper/sapphire interface inside the copper block. For the calibration it is assumed that the surface temperature of the sapphire window is the same as measured in the copper block. The calibration is repeated for the surface temperatures from 80 °C up to 380 °C in steps of 10 °C for each camera setting. The recorded radiance show a perfect agreement with the Stefan-Boltzmann law.

The heat flux at the substrate interface is then obtained by a numerical solution of the heat conduction problem in the sapphire substrate, satisfying the boundary conditions for the evolution of the temperature distribution obtained from the thermographic measurements.

Spray cooling setup. The experimental setup, as shown in Fig. 6c, consists of a heated target, a spraying system, a high-speed visual observation system and a spray characterization system. The target is heated in the beginning of the

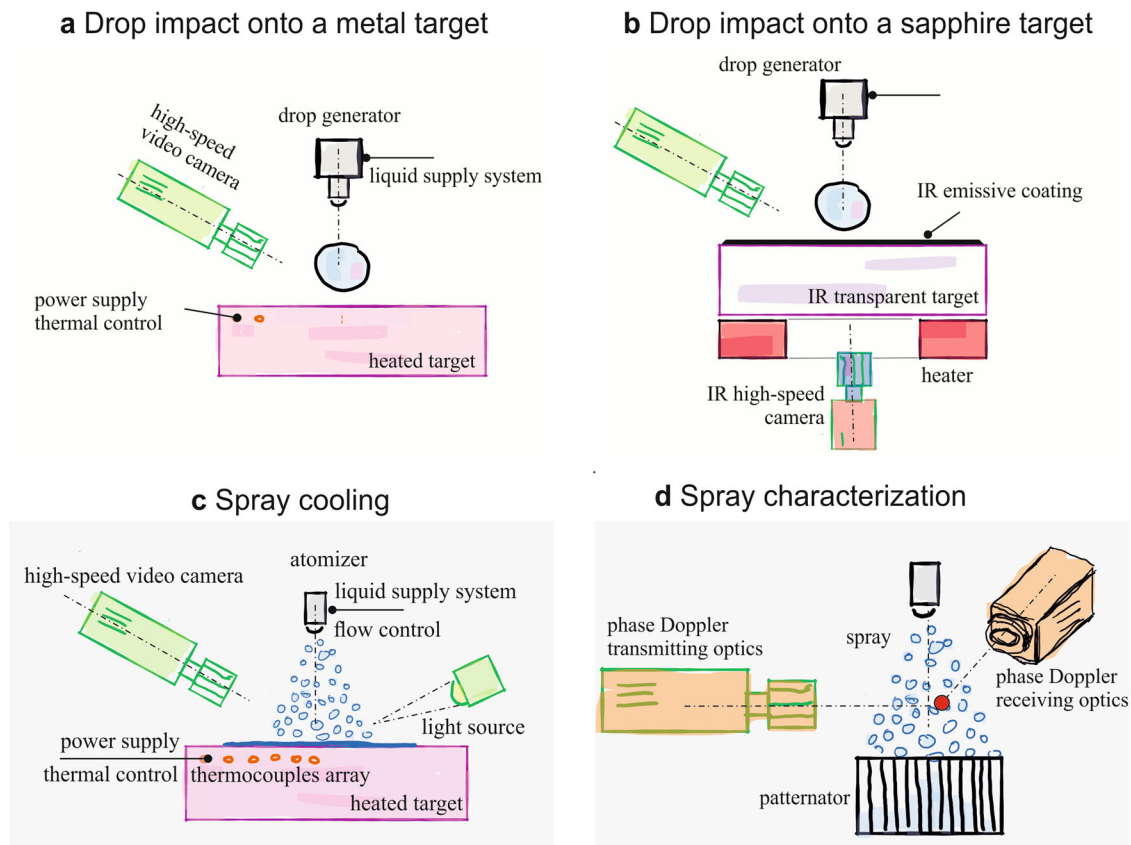


Fig. 6 Sketches of the experimental setups for the single drop and spray cooling experiments. **a** The setup consists of an adjustable drop generation unit, a heated impact target and a high-speed observation system. The heater and impact target are replaced for IR measurements during the drop impact. **b** The setup for infrared (IR) measurements. The heater provides bottom view optical access for a high-speed infrared camera. **c** Setup for characterization of spray cooling. **d** Setup for detailed spray characterization.

experiments with a custom cartridge heater to a surface temperature of 450 °C. After the temperature field inside the target was in steady state, the heater was switched off and a spray was applied to the target surface, until the surface temperature was cooled down to 100 °C. The temperature distribution in the target is measured by a set of 15 thermocouples type K, (class 1), thickness 0.5 mm, placed in two rows at 0.5 mm and 20 mm below the surface. These temperatures are used for computation of the local heat flux and instantaneous surface temperature by solution of the inverse heat conduction problem³⁰. A Phantom v2012 high-speed camera equipped with a long distance microscope (Questar QM-100) allows observation of the hydrodynamic phenomena at the target surface during spray impact. The results of an exemplary experiment is shown in Fig. 3.

Different standard pressure driven full-cone nozzles have been used to vary and identify the effect of the main spray parameters on the cooling rate. The average drop diameter, average velocity and the mass flux density of the spray have been varied in the experiments and accurately characterized using a Dantec phase Doppler system and a custom built patternator, as schematically shown in Fig. 6d. The phase Doppler measurements were performed without the target, but at positions corresponding to specific locations immediately above the target; hence the spray parameters were local values.

To determine the effect of the wall thermal properties on the threshold temperature T^* , two targets of different materials, stainless steel (1.4841) and nickel (2.4068) have been used. The surface roughness is in the same order of magnitude as in the single drop experiments with a polished surface (surface roughness $S_a = 0.0092 \mu\text{m}$).

The substrate materials and their thermal properties. The experimental data from the literature, the substrate materials and their thermal properties are summarized in Table 1. The thermal properties of the designated substrate materials are taken from general literature and handbooks. Since these properties are temperature dependent, they have been calculated at the corresponding threshold temperature. In all cited studies the surfaces are polished.

For the threshold temperature T^* during spray cooling the point corresponding to the minimum heat flux is taken.

Data availability

The data sets for the residence time of the single drop, threshold temperature for low-speed drop impact and spray cooling, presented in this manuscript, are available online in TUDatalib (<https://doi.org/10.48328/tudatalib-530>)³¹.

Received: 9 August 2020; Accepted: 14 July 2021;

Published online: 13 August 2021

References

- Bertola, V. An impact regime map for water drops impacting on heated surfaces. *Int. J. Heat Mass Transf.* **85**, 430–437 (2015).
- Liang, G. & Mudawar, I. Review of spray cooling – Part 2: High temperature boiling regimes and quenching applications. *Int. J. Heat Mass Transf.* **115**, 1206–1222 (2017).
- Breitenbach, J., Roisman, I. V. & Tropea, C. From drop impact physics to spray cooling models: a critical review. *Exp. Fluids* **59**, 55 (2018).
- Roisman, I. V., Rioboo, R. & Tropea, C. Normal impact of a liquid drop on a dry surface: model for spreading and receding. *Proc. R. Soc. London Ser. A-Math. Phys. Eng. Sci.* **458**, 1411–1430 (2002).
- Yarin, A. L., Roisman, I. V. & Tropea, C. *Collision Phenomena in Liquids and Solids* (Cambridge University Press, 2017).
- Roisman, I. V. Inertia dominated drop collisions. II. An analytical solution of the Navier–Stokes equations for a spreading viscous film. *Phys. Fluids* **21**, 052104 (2009).
- Senoner, J.-M., Castanet, G., Caballina, O. & Villedieu, P. Modeling of water drop impactions in the Leidenfrost regime. *Atom. Sprays* **26**, 853–888 (2016).
- Renardy, Y. et al. Pyramidal and toroidal water drops after impact on a solid surface. *J. Fluid Mech.* **484**, 69–83 (2003).
- Bird, J. C., Dhiman, R., Kwon, H.-M. & Varanasi, K. K. Reducing the contact time of a bouncing drop. *Nature* **503**, 385–388 (2013).

10. Liu, Y. et al. Pancake bouncing on superhydrophobic surfaces. *Nat. Phys.* **10**, 515–519 (2014).
11. Richard, D., Clanet, C. & Quéré, D. Contact time of a bouncing drop. *Nature* **417**, 811–811 (2002).
12. Willis, K. & Orme, M. Binary droplet collisions in a vacuum environment: an experimental investigation of the role of viscosity. *Exp. Fluids* **34**, 28–41 (2003).
13. Roisman, I. V. Fast forced liquid film spreading on a substrate: flow, heat transfer and phase transition. *J. Fluid Mech.* **656**, 189–204 (2010).
14. Itaru, M. & Kunihide, M. Heat transfer characteristics of evaporation of a liquid droplet on heated surfaces. *Int. J. Heat Mass Transf.* **21**, 605–613 (1978).
15. Abu-Zaid, M. An experimental study of the evaporation characteristics of emulsified liquid droplets. *Heat Mass Transf.* **40**, 737–741 (2004).
16. Breitenbach, J., Roisman, I. V. & Tropea, C. Drop collision with a hot, dry solid substrate: heat transfer during nucleate boiling. *Phys. Rev. Fluids* **2**, 074301 (2017).
17. Lee, S.-H. et al. Drop impact on hot plates: contact times, lift-off and the lamella rupture. *Soft Matter* **16**, 7935–7949 (2020).
18. Mertens, S. & Moore, C. Continuum percolation thresholds in two dimensions. *Phys. Rev. E* **86**, 061109 (2012).
19. Quéré, D. Non-sticking drops. *Rep. Prog. Phys.* **68**, 2495–2532 (2005).
20. Feller, W. *An Introduction to Probability Theory and its Applications*, Vol 2 (John Wiley & Sons, 2008).
21. Tenzer, F. M., Roisman, I. V. & Tropea, C. Fast transient spray cooling of a hot thick target. *J. Fluid Mech.* **881**, 84–103 (2019).
22. Staszal, C. & Yarin, A. L. Exponential vaporization fronts and critical heat flux in pool boiling. *Int. Commun. Heat Mass Transf.* **98**, 171–176 (2018).
23. Roisman, I. V., Breitenbach, J. & Tropea, C. Thermal atomisation of a liquid drop after impact onto a hot substrate. *J. Fluid Mech.* **842**, 87 (2018).
24. Zuber, N. On the stability of boiling heat transfer. *Trans. Am. Soc. Mech. Engrs.* **80**, 711–720 (1958).
25. Kakac, S. & Bon, B. A review of two-phase flow dynamic instabilities in tube boiling systems. *Int. J. Heat Mass Transf.* **51**, 399–433 (2008).
26. Aursand, E., Davis, S. H. & Ytrehus, T. Thermocapillary instability as a mechanism for film boiling collapse. *J. Fluid Mech.* **852**, 283–312 (2018).
27. Spiegler, P., Hopfenfeld, J., Silberberg, M., Bumpus, C. F. & Norman, A. Onset of stable film boiling and the foam limit. *Int. J. Heat Mass Transf.* **6**, 987–989 (1963).
28. Wang, Z., Qu, W., Xiong, J., Zhong, M. & Yang, Y. Investigation on effect of surface properties on droplet impact cooling of cladding surfaces. *Nucl. Eng. Technol.* **52**, 508–519 (2020).
29. Cai, C., Mudawar, I., Liu, H. & Si, C. Theoretical Leidenfrost point (LFP) model for sessile droplet. *Int. J. Heat Mass Transf.* **146**, 118802 (2020).
30. Woodfield, P. L., Monde, M. & Mitsutake, Y. Improved analytical solution for inverse heat conduction problems on thermally thick and semi-infinite solids. *Int. J. Heat Mass Transf.* **49**, 2864–2876 (2006).
31. Schmidt, J. B. et al. Dataset: Thermosuperrepellency of a hot substrate caused by vapour percolation. <https://doi.org/10.48328/tudatalib-530> (2020).
32. Hoogendoorn, C. J. & Den Hond, R. Leidenfrost temperature and heat-transfer coefficients for water sprays impinging on a hot surface. In *IFTH International Heat Transfer Conference*, Vol. 4, 135–138 (Begel House Inc., 1974).
33. Shoji, M., Wakunaga, T. & Kodama, K. Heat transfer from a heated surface to impinging subcooled droplets : heat transfer characteristics in non-wetting region. *Heat Tran. Jpn. Res.* **50**, 716–723 (1984).
34. Ito, T., Takata, Y., Mousa, M. M. M. & Yoshikai, H. Studies on the water cooling of hot surfaces (experiment of spray cooling). *Memoirs Faculty Eng. Kyushu Univ.* **51**, 119–144 (1991).
35. Yao, S. C. & Choi, K. J. Heat transfer experiments of mono-dispersed vertically impacting sprays. *Int. J. Multiphase Flow* **13**, 639–648 (1987).
36. Choi, K. J. & Yao, S. C. Mechanisms of film boiling heat transfer of normally impacting spray. *Int. J. Heat Mass Transf.* **30**, 311–318 (1987).
37. Yao, S. C. & Cox, T. L. A general heat transfer correlation for impacting water sprays on high-temperature surfaces. *Exp. Heat Transfer* **15**, 207–219 (2002).
38. Bernardin, J. D., Stebbins, C. J. & Mudawar, I. Mapping of impact and heat transfer regimes of water drops impinging on a polished surface. *Int. J. Heat Mass Transf.* **40**, 247–267 (1997).
39. Tran, T., Staat, H. J. J., Prosperetti, A., Sun, C. & Lohse, D. Drop impact on superheated surfaces. *Phys. Rev. Lett.* **108**, 036101 (2012).

Acknowledgements

The authors gratefully acknowledge the Deutsche Forschungsgemeinschaft for its financial support in the framework of the project SFB-TRR 75, project number 84292822, and the Industrieverband Massivumformung e.V.

Author contributions

C.T. and I.V.R. conceived the project. J.B.S. and J.B. performed the single drop experiments. J.H. and F.M.T. performed the spray cooling experiments. C.T. was responsible for the scientific coordination of the project. I.V.R. developed theoretical description of the problem. All authors performed the data analysis and participated in writing the manuscript.

Funding

Open Access funding enabled and organized by Projekt DEAL.

Competing interests

The authors declare no competing interests.

Additional information

Correspondence and requests for materials should be addressed to I.V.R.

Peer review information *Communications Physics* thanks the anonymous reviewers for their contribution to the peer review of this work.

Reprints and permission information is available at <http://www.nature.com/reprints>

Publisher's note Springer Nature remains neutral with regard to jurisdictional claims in published maps and institutional affiliations.



Open Access This article is licensed under a Creative Commons Attribution 4.0 International License, which permits use, sharing, adaptation, distribution and reproduction in any medium or format, as long as you give appropriate credit to the original author(s) and the source, provide a link to the Creative Commons license, and indicate if changes were made. The images or other third party material in this article are included in the article's Creative Commons license, unless indicated otherwise in a credit line to the material. If material is not included in the article's Creative Commons license and your intended use is not permitted by statutory regulation or exceeds the permitted use, you will need to obtain permission directly from the copyright holder. To view a copy of this license, visit <http://creativecommons.org/licenses/by/4.0/>.

© The Author(s) 2021